

# PCCP

Accepted Manuscript



This is an *Accepted Manuscript*, which has been through the Royal Society of Chemistry peer review process and has been accepted for publication.

*Accepted Manuscripts* are published online shortly after acceptance, before technical editing, formatting and proof reading. Using this free service, authors can make their results available to the community, in citable form, before we publish the edited article. We will replace this *Accepted Manuscript* with the edited and formatted *Advance Article* as soon as it is available.

You can find more information about *Accepted Manuscripts* in the [Information for Authors](#).

Please note that technical editing may introduce minor changes to the text and/or graphics, which may alter content. The journal's standard [Terms & Conditions](#) and the [Ethical guidelines](#) still apply. In no event shall the Royal Society of Chemistry be held responsible for any errors or omissions in this *Accepted Manuscript* or any consequences arising from the use of any information it contains.

## Control of recombination rate by changing the polarity of the electrolyte in Dye-sensitized Solar Cells

Jesús Idigoras,<sup>a</sup> Ramón Tena-Zaera<sup>b</sup> and Juan A. Anta<sup>a</sup>,

Recombination in Dye-sensitized Solar Cells (DSC) is an electron transfer process critical for high efficiency. The chemical nature of the electron acceptor is known to have an important impact on recombination and, hence, limits the choice of hole conductors in DSC and related solar cells. In this respect, Room Temperature Ionic liquids (RTIL) have been recognized as an alternative to volatile organic solvents due to their negligible vapor pressure, which offers the chance for long-term stability. However, RTIL-based electrolytes lead to lower performance, a feature that has been attributed to the high viscosity of ionic liquids and the mass-transport limitation associated with it. In this work we show that the origin of the lower performance is also related to an increase in the recombination loss due to the polar nature of the RTIL and the influence of the reorganization energy of the electron acceptor in a polar environment. To investigate this chemical effect, different mixing ratios of RTIL and an organic solvent (acetonitrile) have been considered. The fabricated devices have been characterized by small-perturbation techniques (Impedance Electrochemical Spectroscopy, Intensity-Modulated Photovoltage and Photocurrent Spectroscopies) and Open-Circuit Voltage Decays, which have been used to extract electron lifetimes at different applied voltages. Two different Ruthenium dyes (hydrophilic N719 and hydrophobic Z907) and two different cations in the RTIL (Imidazolium- and Pyrrolidinium-based) have been considered. The results obtained show that for pure ionic liquids the lifetime-voltage curve is exponential, which is a signature of large reorganization energies for electron transfer. In contrast, pure acetonitrile exhibits a non-exponential behavior, which is consistent with a relatively small reorganization energy. Interestingly, and as a general rule, we find that recombination is faster in systems with higher reorganization energies. This is interpreted as a consequence of the availability of more acceptor states for electron transfer. In addition, it is found that mixing RTIL and acetonitrile is an interesting strategy to increase the stability of DSC without significant recombination losses, provided that the right dye and RTIL, in particular a pyrrolidinium component, is used.

### Introduction

Dye-Sensitized Solar cells (DSC) have been recognized as an interesting alternative to conventional silicon photovoltaic cells.<sup>1-3</sup> Their low manufacturing cost and high-energy conversion efficiency

<sup>a</sup> Área de Química Física, Departamento de Sistemas Físicos, Químicos y Naturales, Universidad Pablo de Olavide, E-41013, Sevilla, Spain.

<sup>b</sup> Energy Division, IK4-CIDETEC, Parque Tecnológico de San Sebastián, Paseo Miramón 196, Donostia-San Sebastián 20009, Spain.

made them one of the most promising energy sources. Furthermore, they represent the concept from which the very recent and promising technology of perovskite solar cells emerged.<sup>4</sup> In a DSC sunlight is converted to electricity through light absorption by a dye molecule anchored to semiconductor metal oxide nanostructured films. After photoexcitation of the dye, electron injection from the dye to the semiconductor takes place. By electron diffusion, the injected electron travels through

nanoparticles and is collected in an external circuit. At the same time, the dye has to be regenerated by the reduced form of the redox pair in the electrolyte, which generates a hole that migrates and is reduced at the counterelectrode. This pathway completes the electron cycle. However, several reactions such as internal conversion in the excited dye and electron recombination from the semiconductor to the oxidized dye or to the redox couple in the electrolyte bring about an efficiency loss. It is important to mention that all these processes are determined by the semiconductor/dye/electrolyte interface,<sup>5–8</sup> which plays a critical role in the functioning of DSC and related devices.

An energy conversion efficiency of 13% has been reported<sup>9</sup> thanks to a novel dye-electrolyte combination that minimizes recombination. However, the use of volatile solvents endangers long-life devices as a consequence of losses by leakage and evaporations. Due to concerns about the long-term stability of DSC, there has been a great interest in finding a substitute for volatile electrolytes based on organic solvents. During the last decade, Room Temperature Ionic Liquids (RTIL) have been investigated as alternative solvents in DSC due to their appealing properties for DSC applications, that is, wide electrochemical windows, thermal stability, extremely low volatility or negligible vapor pressure, high ionic conductivity and ability to dissolve organic and inorganic compounds. However, the viscosity of typical RTIL is about 100 times higher than the viscosity of acetonitrile, a fact that has been used to explain the lower performance of RTIL-based DSC. However, high recombination rates have systematically been reported for these electrolytes.<sup>10</sup> In spite of that, conversion efficiencies of around 9% have been reported for ionic liquid-based DSC.<sup>11</sup> Indeed, the recent 300 m<sup>2</sup> solar façade of the Swiss Tech Convention Center (Lausanne, Switzerland), which can be considered the first real architectural integration of this technology, is based on RTIL-based DSC, demonstrating their potential in Building Integrated Photovoltaics (BIPV) applications. The origin of the high recombination rate and a systematic study of the fundamental impact of the chemical nature of the electrolyte on the electron transfer reaction in DSC are still lacking. In this respect, a recent report by us<sup>12</sup> pointed to the importance of ligand (inner) and solvent (outer) interactions and the polarity of the solvent in the recombination rate.

The electron recombination rate ( $U_n$ ) is determined by the energetics of electrons in the semiconductor, mediated by the distribution of localized states, and by the energetics of electron acceptors, which depends on the chemical composition of the electrolyte. To describe these losses, the following equation for the recombination rate can be solved<sup>13,14</sup>

$$U_n = d \int g(E) f(E - E_F) P_R(E) dE \quad (1)$$

where  $d$  is the film thickness,  $g(E)$  is the density of localized (donor) states (usually an exponential function),  $f(E - E_F)$  is the occupation probability in the semiconductor at a certain position of the electron quasi-Fermi level  $E_F$  (Fermi-Dirac distribution), and  $P_R(E)$  is the probability of recombination at a given value of the energy (density of acceptor states). For one-electron outer sphere redox couples,  $P_R(E)$  can formally be described by the Marcus-Gerischer model.<sup>15,16</sup> This factor depends on the concentration of oxidized species in the electrolyte, the redox potential of the electrolyte ( $E_{redox}$ ) and the reorganization energy  $\lambda$ . The reorganization energy is a strong function of the chemical environment, as it depends on the interactions between charged species and the surroundings, composed of solvent and dye molecules.<sup>12</sup> For instance, it is known

that for polar solvents the reorganization energy is larger, due to strong polar interaction between ions and solvent molecules.<sup>15</sup> As a matter of fact, it is found that when  $\lambda \gg E_F - E_{redox}$ , Eq. (1) leads to an exponential dependence of the lifetime with respect to voltage.<sup>13,17</sup> In contrast, a relatively low value of the reorganization energy leads to a departure from the exponential law, and the appearance of a minimum due to the depletion of acceptor states as the Fermi level is raised.<sup>18</sup>

On the other hand, in the search for new RTIL, it has to be taken into account that their physical and chemical properties depend on the interactions between the cations (imidazolium, pyridinium, alkylammonium or pyrrolidinium) and the anions (dicyanamide, thiocyanate or tetracyanoborate, among others). Imidazolium have been the most used component of solvent-free electrolytes in DSC. However, several investigations revealed significant influence of the RTIL composition upon processes relevant to the overall dynamic of DSC, such as electron injection yield,<sup>19,20</sup> electron lifetimes<sup>21</sup> and the rate of regeneration of the oxidized dye.<sup>22</sup> Additionally, the nature of the RTIL can also affect the electron diffusion coefficient in the photoanodes due to the electrical coupling with counterion charges in the electrolyte.<sup>23,24</sup>

The aim of this work is two-fold. On the one hand (1), we intend to cast some light on the mechanism of electron recombination in DSC taking into account the polar nature of the RTIL, which can be tuned by mixing with an organic solvent such as acetonitrile. In this respect, we intend to gain a deeper insight into the findings of a previous work by us,<sup>12</sup> where exponential and non-exponential lifetimes were found depending on the composition of the electrolyte. On the other hand (2), we have investigated the capability of hybrid electrolytes composed of mixtures of RTIL with a low-viscosity and low-polarity solvent as acetonitrile to achieve good performing cells with non-volatile solvents and small mass-transport limitations. It has already been shown by Yu and coworkers<sup>25</sup> that “incompletely solvated ionic liquid mixtures” are very stable under light soaking conditions. In this work we show that the RTIL/organic solvent combination, for small quantities of organic solvent, is not only beneficial in terms of stability, but also in terms of reduced recombination.

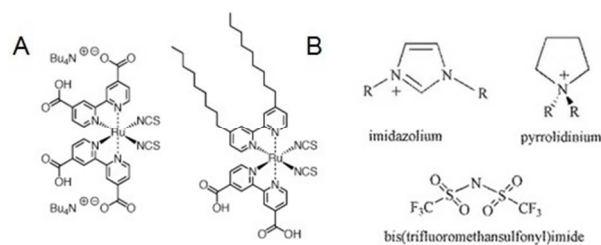


**Fig. 1:** Structures of dye molecules used in this work: (A) N719 and (B) Z907; and Room Temperature Ionic Liquids employed as solvents (C): imidazolium (imid) and pyrrolidinium (pyr)

In this line, two different dyes (hydrophilic N719 and hydrophobic Z907) and two RTIL with two different cations (imidazolium and pyrrolidinium) have been used as components in the polar/apolar mixed DSC electrolytes (Fig. 1). The influence of the RTIL/acetonitrile mixing ratio on photovoltaic performance and the recombination kinetics has been investigated by voltammetry, Electrochemical Impedance Spectroscopy (EIS), Intensity-Modulated Photovoltage and Photocurrent Spectroscopies (IMVS/IMPS) and Open-Circuit Voltage Decays (OCVD).

## Results and discussion

### Photovoltaic performance

Figure 2 shows current-voltage characteristics of cells employing the N719 as sensitizer for the studied electrolytes. To test the reproducibility of the results, four cells were fabricated for each composition, and no significant deviations were found between them. The photovoltaic parameters (short-circuit current density ( $J_{sc}$ ), open-circuit voltage ( $V_{oc}$ ), fill factor and power conversion efficiency ( $\eta$ )) for each configuration are given in Table 1.

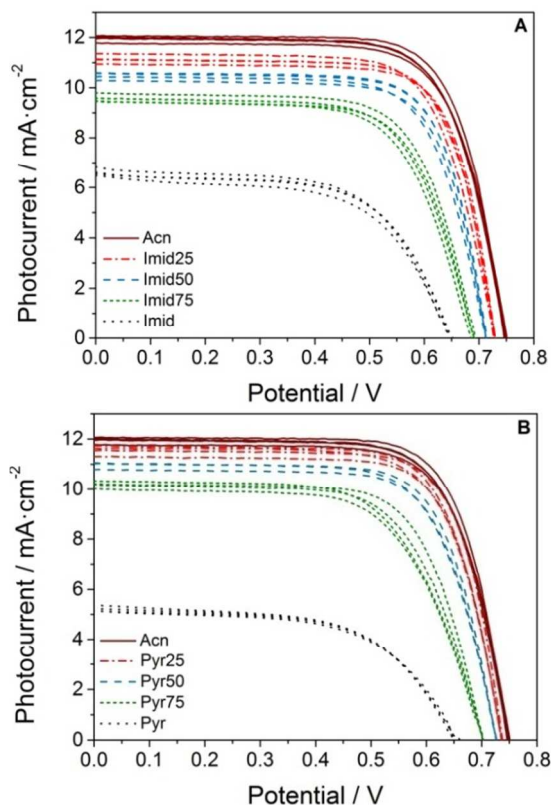


Fig. 2: Current-voltage curves under 1-sun AM1.5 for different RTIL/Acn mixing ratios. Results for both used ionic liquids are shown: A) Imid and B) Pyr.

Electrolyte	$J_{sc}$ ( $\text{mA}\cdot\text{cm}^{-2}$ )	$V_{oc}$ (mV)	Fill Factor	Efficiency ( $\eta$ )
Acn	12.1	745	74	6.6
Imid25	11.5	728	74	6.0
Imid50	10.6	712	73	5.6
Imid75	9.7	690	69	4.7
Imid	6.8	650	60	2.8
Pyr25	11.8	735	73	6.2
Pyr50	11.0	727	72	5.8
Pyr75	10.2	702	68	4.9
Pyr	5.3	655	57	2.0

Table 1: Photovoltaic parameters measured under simulated AM 1.5 sun illumination of the best DSC for each electrolyte composition and employing the N719 dye.

The maximum efficiency (6.6%) was found for the pure acetonitrile-based electrolyte. This good efficiency is achieved by a proper combination of additives, which maximize open-circuit photovoltage (745 mV), fill factor (74%) and photocurrent ( $12.1 \text{ mA}\cdot\text{cm}^{-2}$ ). The electrolyte composition used is very similar to the best-performing electrolyte employed in Ref. [12]. To compensate the high viscosity of the ionic liquids a higher concentration of iodine (0.1M) was used. The increment of the concentration of  $\text{I}_3^-$  can lead to a lower performance of the cell. It must be born in mind that iodine absorbs light, which produces a diminution of the photocurrent.<sup>26</sup> In addition, an increase in the iodine concentration can accelerate the recombination since more tri-iodide ions are available for accepting electrons. Nevertheless, efficiencies of 2.8% and 2.0% were obtained for pure Imid and Pyr, respectively. Importantly, efficiencies around 5% are obtained for the mixtures where the RTIL is the majority component. This efficiency is comparable to that reported by Yu et al.<sup>25</sup> for a similar composition. The relative high viscosity of Imid and Pyr (35.55cP and 85.33cP at 298K, respectively), which are about several orders of magnitude higher than the viscosity of acetonitrile (0.34cP at 298K),<sup>27</sup> appears to limit their efficiency due to severe mass-transport limitations<sup>26,28</sup> related to their ionic diffusion coefficients. This has been confirmed by measuring cyclic voltammograms in blank cells (Fig. 3). Consequently, the efficiency of regeneration of the oxidized dye by the reduced form of the redox couple is limited. These limitations, which are primarily reflected in the  $J_{sc}$  and in the fill factor, are reduced as more acetonitrile is added to the RTIL. Therefore, the photovoltaic parameters are improved. However, it is noteworthy that adding just a 25% in volume of acetonitrile doubles the short-circuit photocurrent and the efficiency. This effect is more pronounced for Pyr-based electrolytes than for Imid-based electrolyte (see Supporting Information, Fig. S1). Hence, the addition of acetonitrile (25% in volume) into Imid and Pyr produces an increase in the  $J_{sc}$  of 42% and 92% respectively. In order to be sure that the observed effect does not depend on the used dye, another ruthenium sensitizer, Z907, was employed, which yielded similar results to those obtained with the N719 dye (see Supporting Information, Fig. S2).

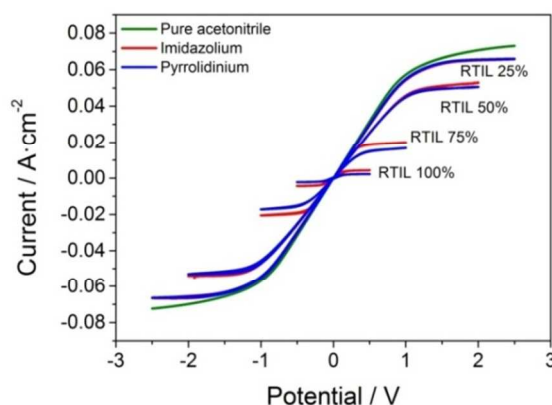


Fig. 3: Cyclic voltammetry of Pt@FTO/ Pt@FTO (blank cells) for all RTIL/Acn mixing ratios.

It is very important to point out that the benefit of using Pyr versus Imid has nothing to do with a lower transport limitation, as the limiting currents of Pyr/Acn and Imid/Acn electrolytes with the same mixing ratio are very similar (Fig. 3), in spite of Pyr being even slightly more viscous. Furthermore, the overall improvement in performance as more acetonitrile is added is not only observed in

short-circuit photocurrents and fill factors, but also in the open-circuit voltage, when no current is running through the device. This observation indicates that the origin of the lower performance of RTIL electrolytes is not due to transport limitations only. This issue is further investigated in the following sections.

### Electrochemical impedance spectroscopy.

EIS Nyquist plots at the OC photovoltage are presented in Figure 4 for all Pyr-based N719 DSC. The spectra show the characteristic three semicircles typically observed in DSC.<sup>10,29</sup> The high-frequency one is related to charge transfer at the platinum counter-electrode, the one at mid frequencies arises from electronic processes at the oxide/electrolyte interface and the semicircle appearing at low frequencies reflects the diffusion of redox species in the electrolyte. This semicircle only appears in the most viscous electrolytes (high RTIL/Acn mixing ratio) due to the mass-transport limitation in the electrolyte.

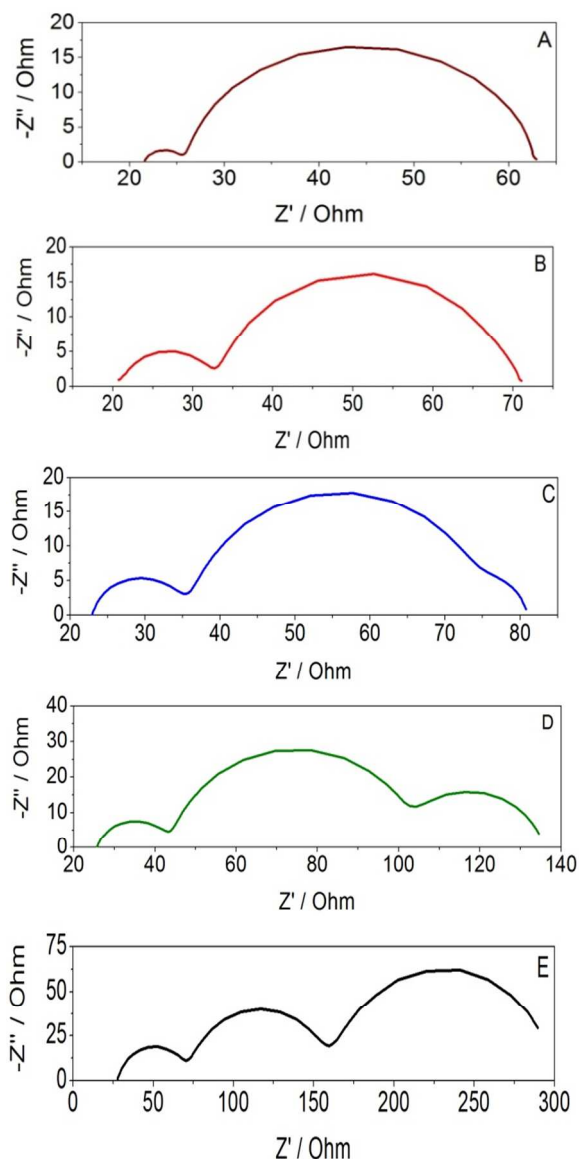


**Fig. 4:** EIS Nyquist plots for all Pyr-based electrolytes and acetonitrile in N719-cells at the different ratio RTIL/Acn: A) Acn, B) Pyr25, C) Pyr50, D) Pyr75 and E) Pyr. All these spectra have been measured under illumination and at the open-circuit photovoltage of each cell at 1 sun

The EIS results can be well fitted to the diffusion-recombination model of Bisquert and coworkers<sup>29,30</sup> (see Supporting Information, Fig. S3). However, it has to be noted that it was not possible to fit to the simple diffusion-recombination equivalent circuit for cells with pure RTIL, possibly due to the short electron diffusion length, as discussed below. Furthermore, this equivalent circuit was not found suitable at low potentials either ( $< 0.55$  V). As it is in this regime where direct electron transfer between the FTO substrate and the electrolyte becomes significant,<sup>30,31</sup> we attribute this problem to the lack of additional circuit elements, as indicated in Ref.[30]. However, as said, the diffusion-recombination model works well at moderate and high potentials, which is the region of interest for cell operation. The region of low potentials is better explored with the OCVD technique, although with limitations, as explained below.

The fittings allow extracting the electron lifetime via

$$\tau_n = R_{rec} C_\mu \quad (2)$$

where  $R_{rec}$  and  $C_\mu$  refer to the recombination resistance and the chemical capacitance in the oxide/electrolyte interface, respectively. These two parameters have in typical DSC, and in conditions in which trapping is dominant, a voltage dependence given by<sup>32</sup>

$$R_{rec}^{-1} = \frac{\partial J_R}{\partial E_F} = R_{rec,0}^{-1} \exp\left[\beta(E_F - E_F^0)/k_B T\right] \quad (3)$$

$$C_\mu^{-1} = \frac{\partial E_F}{\partial n} = C_{\mu,0}^{-1} \exp\left[-\alpha(E_F - E_F^0)/k_B T\right] \quad (4)$$

where  $k_B$  is Boltzmann constant,  $T$  is the absolute temperature,  $\beta$  is a dimensionless parameter which can be related to the reaction order of the recombination reaction with respect to free electrons<sup>33</sup> and  $\alpha$  is a dimensionless parameter related to the mean energy of the exponential distribution of localized states in the oxide  $g(E)$ .<sup>34</sup> In Eqs. (3) and (4), the voltage difference acting in the device (assuming no voltage drop in the substrate/oxide and in the electrolyte/counter-electrode interfaces) corresponds to the difference in Fermi level in the oxide and in the electrolyte, i.e.  $V = E_F - E_F^0$ . As a general observation, electron recombination resistance and capacitance data for the studied cells fit quite well to Eqs. (3) and (4), although small departures from the exponential law are detected for  $C_\mu$  at lower voltages. In Figure S4 in the Supporting Information, the chemical capacitance extracted from EIS analysis at different potentials is shown. The EIS results show that the capacitance is not altered by the RTIL/Acn mixing ratio, which indicates that, probably as a consequence of using the same additives in all electrolytes, no significant shifts of the conduction band are occurring. Therefore, taking into account Eq. (2), the electron lifetime is mainly determined by the electron recombination resistance at the  $\text{TiO}_2$ /electrolyte interface. In Figure 5, electron recombination resistances and electron lifetimes using both RTIL are shown for all the RTIL/Acn mixing ratios considered in this work.

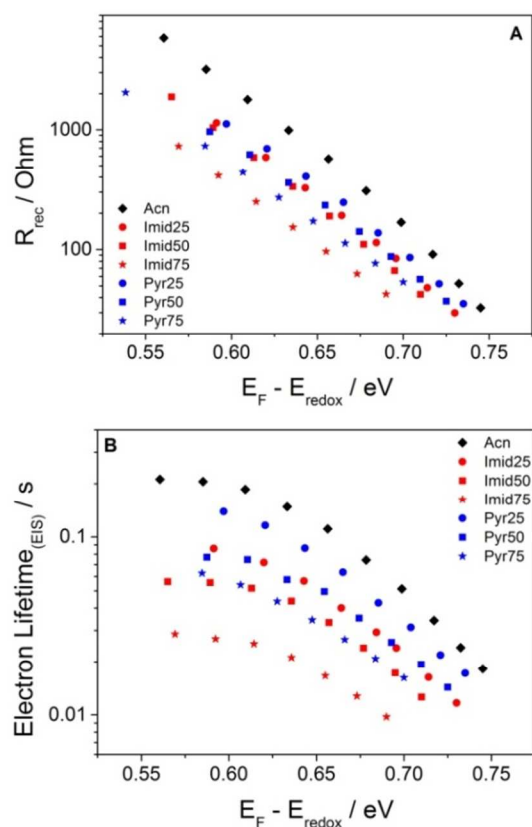


**Fig. 5:** (A) Electron recombination resistance and (B) electron lifetime data are extracted from EIS measurement in N719-cells.

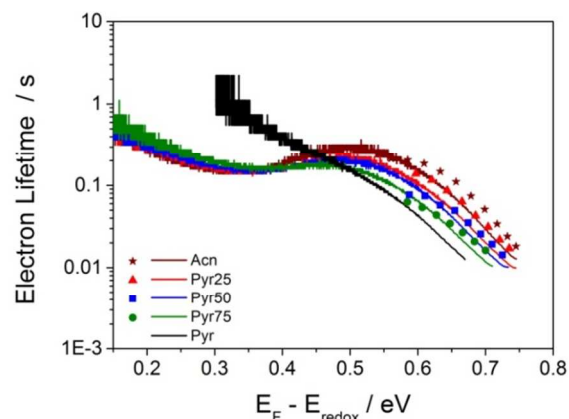
Figures 4 and 5 show a systematic increase of the recombination resistance and of the electron lifetime when the RTIL/Acn mixing ratio is reduced, which explains the improvement of the photovoltage with respect to pure RTIL. Consequently, cells with pure acetonitrile in the electrolyte show the highest  $V_{oc}$ . Furthermore, it is important to stress that the results obtained point to a more intense blocking of electron recombination with tri-iodide ions by pyrrolidinium cations than by imidazolium ones. Similar results were obtained in Z907-cells (see Supporting Information, Fig. S5). In conclusion, the cells with Pyr-based electrolytes show better performance than with Imid-based electrolytes in spite of being a slightly more viscous ionic liquid. However, solar cells containing Pyr show, systematically, lower fill factors. This difference can be related to its viscosity and/or a higher charge transfer resistance at the counter-electrode for cells with Pyr-based electrolytes. As can be observed in Figure S6 in the Supporting Information, the semicircle at high frequencies, related to charge transfer at the platinum counter-electrode, features a higher resistance for Pyr than for Imid-based electrolytes.

### Open-circuit Voltage Decays.

The OCVD data provide a simple and ready means of probing the recombination process. A proper interpretation of OCVD data involves the extraction of the lifetime via Eq. 5, which is actually related to the time derivative of the voltage decay.<sup>35</sup>

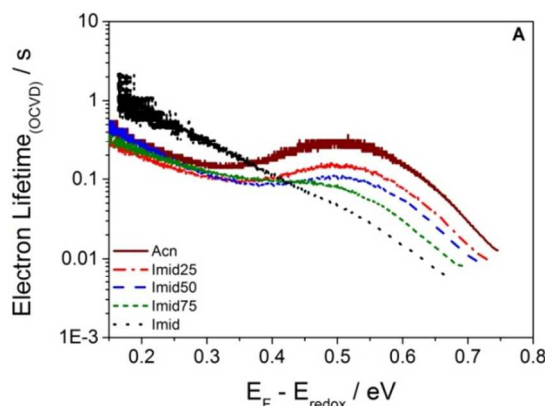
$$\tau_n = \frac{1}{\beta k_B T} \left( \frac{dV_{oc}}{dt} \right)^{-1} \quad (5)$$

In Figure 6 a comparison of electron lifetimes extracted from OCVD and EIS are presented. In general, good agreement between both techniques is accomplished for the studied electrolytes. However, it must be born in mind that OCVD is a dark technique, whereas the EIS lifetimes are obtained under illumination, which may produce small deviations.<sup>5</sup> Electron lifetimes at high voltages from EIS and OCVD exhibit the same behavior and very similar values for all studied electrolytes. At potentials lower than 0.5-0.55 eV, it was not possible to obtain EIS data, as explained above.



**Fig. 6:** Electron lifetimes as extracted from OCVD (lines) and EIS (squares) for Pyr-based electrolytes in N719-cells.

In Figure 7 OCVD lifetimes for different mixing ratios and different dyes (N719 and Z907) are shown. Two main observations can be derived from the results in Figures 6 and 7. First, as discussed in the previous section, the addition of acetonitrile reduces the recombination rate, leading to longer lifetimes. Second, we find that all solar cells with acetonitrile in a major or minor proportion exhibit non-exponential behavior in the lifetime-voltage curve. However, solar cells with pure RTIL yield exponential lifetimes (straight lines in the semilogarithmic plot). This observation suggests that a substantially different recombination mechanism is taking place in the two cases, probably produced by the change in polarity. The origin of this feature is discussed below.



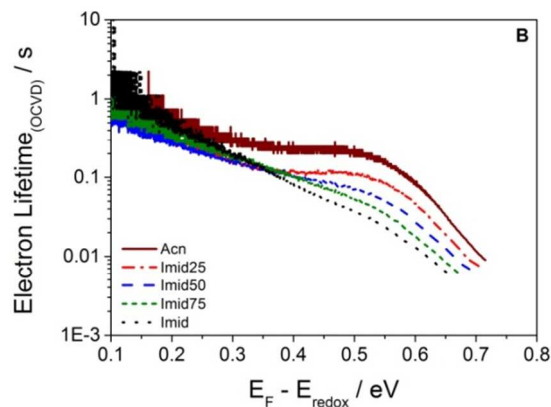


**Fig. 7:** Electron lifetimes as extracted from OCVD for various Imid/Acn mixing ratios in N719-cells (A) and Z907-cells (B).

It is known that OCVD can be affected by charge transfer through the FTO/TiO<sub>2</sub> interface at low potentials. This artifact is commonly prevented by depositing a blocking layer between the FTO and the TiO<sub>2</sub> film.<sup>31</sup> To make sure that the departure from the exponential behavior and the appearance of a minimum for some electrolytes is not due to this artifact we have compared cells with and without blocking layers. The results are presented in the Supporting Information (see Supporting Information, Fig. S7), where it is shown that cells with and without blocking layer, although with slightly smaller lifetimes for the latter, especially in the region of low potentials, exhibit the same features described above. A transition from exponential to non-exponential behavior in the OCVD data for cells with blocking layer has already been reported in Refs. [12] and [18], hence excluding any key influence of the presence of the BL in the shape of the lifetime-voltage plot.

It is known that the addition of a non-volatile component into acetonitrile is appealing in terms of stability. Thus, under light soaking for 1000h, a deterioration of 50% and 80% in efficiency have been reported in DSC containing electrolytes based on pure acetonitrile and on mixed solvents (Acn/RTIL, 2:1 v/v), respectively.<sup>25</sup> However, we have demonstrated that recombination is enhanced in the presence of RTIL. The combination of both facts suggest that an optimized mixture of acetonitrile and RTIL can be interesting for working devices in terms of both stability and low recombination.

As mentioned in the introduction, the total recombination rate for a DSC device can be quantified using the following formula

$$U_n = d \int g(E) f(E - E_F) P_R(E) dE \quad (1)$$

where  $d$ ,  $g(E)$ ,  $f(E - E_F)$  were defined above and  $P_R(E)$  is the probability of recombination at a given value of the energy (density of acceptor states). For one-electron outer-sphere redox couples, this probability can be calculated using the Marcus-Gerischer model

$$P_R(E) = k_r \exp \left[ -\frac{(E - E_{redox} - \lambda)^2}{4\lambda k_B T} \right] \quad (6)$$

where  $\lambda$  is the reorganization energy,  $E_{redox}$  is the redox potential of the redox couple, and  $k_r$  is a prefactor that depends on the concentration of oxidized species in the electrolyte, the temperature and the reorganization energy. The small-perturbation electron lifetime<sup>13</sup> can be obtained from Eq. (1) according to its definition

$$\tau_n = \left( \frac{dU_n}{dn} \right)^{-1} \quad (7)$$

The small-perturbation lifetime is hence defined as the variation of the recombination rate for small variations of the total density. It can be shown,<sup>13</sup> that for an exponential distribution of localized states  $g(E)$ , in the zero-temperature limit of the Fermi-Dirac distribution  $f(E)$  and assuming that  $\lambda \gg (V = E_f - E_{redox})$ , the recombination resistance is given by Eq. (3) and the lifetime, accordingly, by

$$\tau_n = \tau_{dark} \exp \left[ \frac{(\alpha - \beta)V}{k_B T} \right] \quad (8)$$

Hence, an exponential behavior is expected for large reorganization energies. In contrast, a relatively small value of  $\lambda$  implies from Eq. (6) that the probability of electron recombination is reduced if the starting energy  $E$  of electrons is larger than  $E_{redox} + \lambda$  (inverted regime), so that a curvature in the lifetime-voltage plot appears. The observed behavior of the lifetime strongly suggests that the reorganization energy is large for pure and high concentrations of RTIL, whereas for acetonitrile the reorganization energy is smaller. However, the iodide/tri-iodide system is not a one-electron redox couple and the use of the Marcus model to describe electron transfer from TiO<sub>2</sub> is not straightforward. Nevertheless, it has been demonstrated that the dye regeneration process takes place by one-electron transfer.<sup>36</sup> The real electron acceptor has not been clearly identified, although spectroscopic studies suggest that it is tri-iodide.<sup>37</sup> In any case, the recombination reaction necessarily implies the existence of a first step of electron transfer to a species in the electrolyte. This should involve reorganization energy, associated to the interaction with solvent molecules of this species, whatever it is. A quite different polarity of the surrounding medium will critically determine the value of this reorganization term. Furthermore, it is well-known<sup>15</sup> that  $\lambda$  is larger for polar solvents than for non-polar ones. The observed behavior of the electron lifetime is then consistent with this interpretation. Recent reports have shown that the dielectric constant of the RTIL studied in this work do not have, contrary to what is commonly believed, very high dielectric constants.<sup>38</sup> This would indicate that polarity by itself is not the cause of the effect observed in the present study. However, not only the dielectric constant affects the reorganization energy (outer sphere or solvent component<sup>25</sup>) but also the direct chemical interaction between ligands or solvent molecules with the electrochemically active species. In this regard, the ionic nature of the RTIL makes them strongly solvating agents<sup>39</sup> which explains the huge impact on the lifetime-voltage behaviour.

Apart from the different shape in the lifetime-voltage plot, as already pointed out, the increase in the polarity of the solvent is accompanied by an enhancement of the recombination loss. This indicates that a larger value of  $\lambda$  accelerates electron recombination. Assuming that the probability of recombination is determined by the Marcus model, i.e., Eq. (6), a more rapid recombination is explained by the larger availability of acceptor states at higher energies, provided that electrons recombine from high energies as well. The fact that electron recombination takes place from the conduction band, has been considered to explain the behavior of electron lifetimes and diffusion lengths with respect to illumination and addition of Li<sup>+</sup> ions to the electrolyte.<sup>40,41</sup> However, a recombination mechanism *exclusively* via the conduction band does not explain the non-linear features of the recombination rate, i.e., a  $\beta$  coefficient smaller than one<sup>17,33,42</sup> as observed in the present experiments. To account for both non-linear features and the effect of the

composition, we proposed in previous works<sup>12,17</sup> that recombination can take place via: (1) direct electron transfer from localized states in the band gap, and (2) from quasi-free electrons, that get transferred to the electrolyte from high energy levels (Fig. 8). According to this interpretation, a larger value of the reorganization energy leads to an enhancement of process (2) added to process (1), hence explaining the change of shape in the lifetime-voltage plot and the shortening of the lifetime.

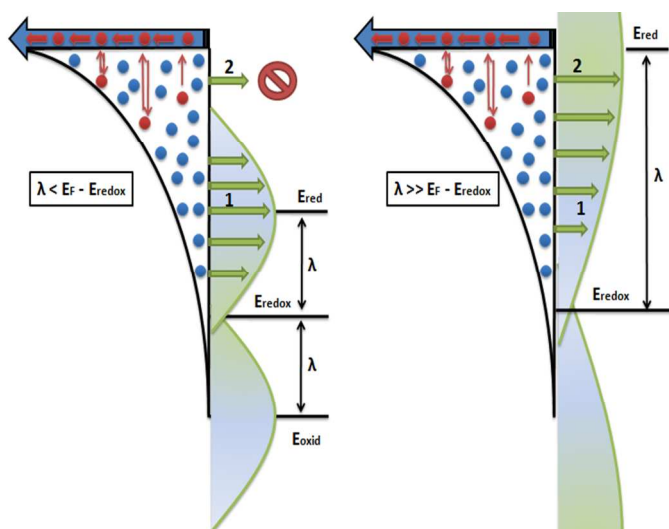


**Fig. 8:** Illustration of the effect of reorganization energy and chemical environment on the recombination kinetics across the oxide/electrolyte interface. Left: redox mediator in weak-interacting chemical environment. Right: redox mediator in a strong-interacting chemical environment. In the figure (1) represents direct recombination from trap states and (2) recombination of quasi-free electrons from states close to the transport level.

To further confirm this interpretation, the model of Ref. [17] has been used to obtain normalized lifetimes for different values of the reorganization energy. The Random Walk Numerical Simulations (RWNS) were performed at room temperature using a simulation box  $20 \times 20 \times 20 \text{ nm}^3$  and an exponential distribution of trap energies  $g(E) = N_t \alpha / k_B T \exp(-\alpha(E - E_c) / k_B T)$  with  $\alpha = 0.43$  and a total density of traps of  $N_t = 10^{21} \text{ cm}^{-3}$ . A multiple-trapping mechanism of transport was assumed for electrons and a probability of electron recombination described by Eq. (6) was considered. Here, we took  $E_{redox} - E_c = 0.95 \text{ eV}$ , where  $E_c$  is the position of the  $\text{TiO}_2$  conduction band. As discussed above, two mechanisms were implemented for electron recombination: (1) direct recombination for electrons immobilized in traps and (2) recombination for electrons that get detrapped and mobile and can recombine from shallow traps (Fig. 8). The relative weight of these two mechanisms is crucial to reproduce the change of behavior observed in the lifetime. For instance, if process (1) is too slow with respect to (2), the increase in the reorganization energy is not accompanied by a reduction of the lifetime, as observed in the experiments. In accordance to this, a ratio of  $k_r(1) / k_r(2) = 10^4$  has been considered between the prefactors  $k_r$  in Eq. (6) for both types of recombination processes. The calculations were arranged to simulate an open-circuit voltage experiment. Hence, 300 electrons were placed at random at  $t = 0$ , and then they are allowed to move between traps and recombine. The total population of electrons is then found to decrease with time. From Eq. (7) a lifetime can be extracted. Further numerical details can be found in Ref. [17].

Results for the lifetime-voltage plots for various values of the reorganization energy are presented in Figure 9. The simulation predicts the change of regime from an exponential trend at large values of  $\lambda$  to a weaker dependence with respect to voltage at low  $\lambda$ 's. Note that in contrast to the simple model of Ref. [18], the simulation does not predict a minimum at  $E_f = \lambda$ . The fact that recombination takes place simultaneously from an ensemble of surface states implies that there is not a clearly defined minimum when  $E_f = \lambda$ . What is clearly seen is that, the increase of the reorganization energy is accompanied by a shortening of the lifetime. For instance, changing  $\lambda$  from 0.4 to 0.6 eV reduces the lifetime by more than one order of magnitude, which is quite similar to the changes observed in the experiment. Hence, the numerical model reproduces qualitatively the experimental behavior of the lifetime when the polarity of the solvent is changed.

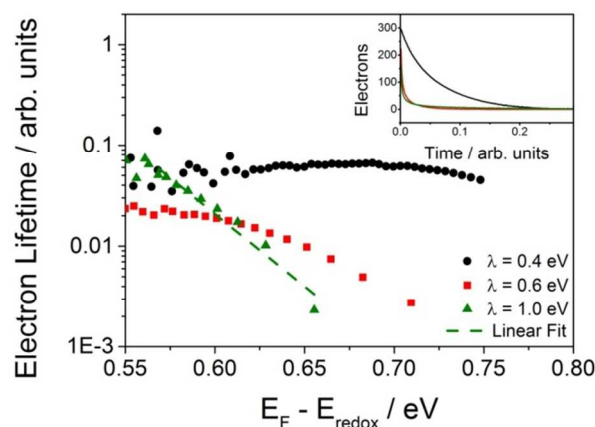
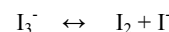


**Fig. 9:** Electron lifetime versus voltage ( $E_f - E_{redox}$ ) as derived from RWNS calculations at different values of the reorganization energy  $\lambda$ . The inset shows the time decay of electron population for the three studied cases.

It has to be mentioned that a different interpretation for the observed trends can be envisioned. As established above, electron recombination is likely to occur with tri-iodide electrons. However, this species is at equilibrium with iodine



The presence of a non-polar solvent will displace this equilibrium to  $(\text{I}_2 + \text{I}^-)$ , hence reducing the effective concentration of tri-iodide and then the recombination rate. However, we do not believe that this is the most likely interpretation, as a displacement of the equilibrium will modify the redox potential of the couple. In fact a positive redox potential shift has been reported for water with respect to methoxypropionitrile.<sup>43</sup> A displacement of the redox potential would produce a shift in the measured chemical capacitances (see Supporting Information, Fig. S4). However, as already discussed, no shift is observed in the capacitance as the RTIL/Acn mixing ratio is varied. Therefore, we infer that the change of both the shape and the absolute value of the lifetime-voltage plots are due to purely kinetic effects rather than to thermodynamic contributions.

To ascertain the origin of the better short-circuit photocurrent for Pyr-based electrolytes, electron diffusion lengths were estimated. This is defined as the average distance that electrons can travel in the photoanode before recombination, hence providing information about charge collection.<sup>33,44,45</sup> For small perturbation of the Fermi level, a small-perturbation diffusion length ( $L_n$ ) can be defined and determined by combining IMVS and IMPS data via the following equation<sup>46,47</sup>

$$L_n = (\tau_n \cdot D_n)^{1/2} \quad (9)$$

where  $\tau_n$  is the lifetime obtained by IMVS<sup>48</sup> and  $D_n$  is the diffusion coefficient obtained by IMPS.<sup>49,50</sup> The pairs of  $\tau_n$  and  $D_n$  used to obtain  $L_n$  must be determined at the same value of the quasi-Fermi level with respect to the conduction band. However, at the same light intensity the position of the quasi-Fermi level is different as in IMVS measurements, which are carried out at open-circuit, and in IMPS measurements, performed at short-circuit. To estimate the shift, a determination of the so-called short-circuit voltage,  $V_{sc}$  is required.<sup>46,51</sup> We obtain values of  $L_n \approx 30$ - $35 \mu\text{m}$  and  $40$ - $50 \mu\text{m}$  for Imid75 and Pyr75 respectively (see Supporting Information, Fig. S8). The difference between these values is a consequence of the more effective blocking of recombination for Pyr, evidenced by the higher electron recombination resistance and electron lifetime. In contrast, the electron transport is similar in both cases. The diffusion coefficients increase exponentially with Femi level,<sup>14,52</sup> as usually observed in DSCs in accordance to the multiple-trapping or hopping models<sup>53,54</sup> in the range between  $10^{-5}$  and  $10^{-3} \text{cm}^2/\text{s}$ , characteristic of nanocrystalline  $\text{TiO}_2$ . However, the values of  $L_n \approx 3d$  and  $4d$  for Imid75 and Pyr75 respectively (where  $d$  is the thickness of film) suggest that the collection efficiency cannot be considered as exactly 100% at short-circuit conditions.<sup>44,55</sup> Hence, the larger value of  $L_n$  for Pyr-based electrolytes points to a higher collection efficiency and therefore to a higher photocurrent at short-circuit.

As with the two RTIL, we have also noticed a different behavior for the two ruthenium dyes N719 and Z907 used to fabricate the solar cells. When the  $\text{I}^-/\text{I}_3^-$  redox couple is present in the electrolyte lower performances are reported in Z907-cells respect to N719 as a consequence of higher recombination losses (see Supporting Information, Fig. S9). The electron lifetimes in N719-cell show a more pronounced departure from the exponential behavior with the appearance of a minimum, whereas in Z907-cells the curves are flatter. According to the interpretation discussed above, higher reorganization energies are expected for Z907-cells, which could explain the higher recombination losses. (It has to be mentioned that in Z907-cells with cobalt complex as redox couple, these faster recombination kinetics is compensated by the standard redox potential, which is 210mV more positive<sup>8</sup> in the case of  $[\text{Co}(\text{byp})_3]^{3+/2+}$  than of  $\text{I}^-/\text{I}_3^-$ ). A possible explanation for the different reorganization energies for both dyes is the presence of two hydrocarbon chains in the Z907 sensitizer. These bulky and apolar groups can modify the local chemical environment of the electron acceptors in the vicinity of the  $\text{TiO}_2$  surface by pushing away acetonitrile molecules, hence increasing the reorganization energy.

## Conclusions

In this work we have carried out a comprehensive study of the photovoltaic performance of acetonitrile/room-temperature-ionic-liquid (RTIL) mixtures in Dye-sensitized solar cells. We have compared two ionic liquids that differ by the nature of the cations that enter their composition (*Imidazolium*- and *Pyrrolidinium*-based) and two ruthenium dyes (N719 and Z907). The electron recombination resistance, chemical capacitance and electron lifetime have been determined as a function of Fermi level position by Impedance Spectroscopy and Open-Circuit Voltage Decay, finding good correspondence between data from both techniques.

The electron lifetime shows two types of behavior: one exhibiting a minimum in the lifetime-voltage plot (acetonitrile), and the other characterized by a pure exponential behavior (RTIL). A progressive transition between both kinds of shape in the lifetime-voltage plot is observed as the acetonitrile/RTIL mixing ratio is

modified. According to previous experimental and theoretical reports, as well as exploratory Random Walk Numerical Simulations carried out here, this behavior of the electron lifetime can be explained by an increase in the value of the reorganization energy for electron recombination as we move from a less polar environment (acetonitrile) to a more polar one. Assuming this interpretation, we reach the important conclusion that systems with large reorganization energies have higher recombination losses, as it is the case in electrolytes based on ionic liquids. We relate these observations with the existence of two electron recombination routes, one produced from deep traps and the other mediated by shallow traps, in such a way that a large reorganization energy allows for a larger contribution of this second route, hence reducing the lifetime.

Interestingly, the change of behavior in the lifetime-voltage plot for pure ionic liquids is produced by solvation with only a minor fraction of acetonitrile. Hence, ionic liquids solvated with relatively small amounts of organic solvents are not only an interesting electrolyte formulation in DSC due to a diminution of the mass-transport limitation, but also due to the decrease of the electron recombination rate (as a result of the reduction of reorganization energy). Furthermore, according to the results here presented, we have also found that the reorganization energy is not only determined by polarity of the solvents, but also by the dye used.

Finally, it is important to point out that the nature of the cation of the RTIL is also critical when it comes to reduce the electron recombination. In this respect pyrrolidinium cations show a much better performance than the more commonly used imidazolium. As a consequence of the blocking of recombination, not only an increase in  $V_{oc}$  is observed, but also an enhancement of  $J_{sc}$  (consequence of a not too long diffusion length). This finding may open opportunities for the application of pyrrolidinium-based RTIL, largely used in batteries, in the DSC field.

## Experimental

### Fabrication of Dye-sensitized Solar Cells

For optimized cell efficiencies, devices were made using  $12 \mu\text{m}$  thick films consisting of a layer of  $8 \mu\text{m}$  of  $20 \text{nm}$   $\text{TiO}_2$  nanoparticles (*Dyesol*® *paste*) and a layer of  $4 \mu\text{m}$  of  $400 \text{nm}$   $\text{TiO}_2$  particles (scattering layer).<sup>56</sup> Prior to the deposition of the  $\text{TiO}_2$  paste the conducting glass substrates (Hartford Glass inc. with  $15 \Omega \text{cm}^{-2}$  resistance) were immersed in a solution of  $\text{TiCl}_4$  (40 mM) for 30 minutes at  $70^\circ\text{C}$  and then dried. For some of the devices (*control cells*), and to prevent recombination of electrons from the glass substrates with the oxidized species in the electrolyte a thin insulating layer (called a *blocking layer*) was placed between the mesoporous oxide and the substrate. This thin film was prepared by spin coating from the following solution: 20ml of  $\text{H}_2\text{O}$  MilliQ + 2.2ml of Titanium (IV) isopropoxide + 1.5ml of Acetylacetone. After deposition, the substrate was heated to  $500^\circ\text{C}$ . The  $\text{TiO}_2$  nanoparticle paste was deposited onto a conducting glass substrate using the screen printing technique. The DSC active area was  $0.16 \text{cm}^2$ . The  $\text{TiO}_2$  electrodes were gradually heated under airflow at  $325^\circ\text{C}$  for 5 min,  $375^\circ\text{C}$  for 5 min,  $450^\circ\text{C}$  for 15 min and  $500^\circ\text{C}$  for 15 min. The heated  $\text{TiO}_2$  electrodes were immersed again in a solution of  $\text{TiCl}_4$  (40 mM) at  $70^\circ\text{C}$  for 30 min and then washed with water and ethanol. Finally, the electrodes were heated again at  $500^\circ\text{C}$  for 30 min and cooled before dye adsorption.

The counter-electrode was made by spreading a 10 mM solution of  $\text{H}_2\text{PtCl}_6$  in ethanol onto a conducting glass substrate with a small

hole to allow the introduction of the liquid electrolyte using vacuum, followed by heating at 390 °C for 15 minutes.

The electrodes were immersed overnight in a solution containing ruthenium dyes coded **N719** (*cis-diisothiocyanato-bis(2,2'-bipyridyl-4,4'-dicarboxylato) ruthenium(II) bis (tetrabutylammonium)*) and **Z907** (*cis-diisothiocyanato-(2,2'-bipyridyl-4,4'-dicarboxylic acid)-(2,2'-bipyridyl-4,4'-dinonyl) ruthenium(II)*). These solutions were composed of 0.3mM dye and 0.3mM chenodeoxycholic acid in ethanol. The sensitized electrodes were washed with ethanol and dried in air. Finally, the working- and counter-electrodes were sandwiched together using a thin thermoplastic frame (Surlyn, Solaronix) that melts at 100 °C. The cells were filled with the electrolyte through a hole previously made in the back of a platinized counter electrode. Then, the hole was sealed with a thermoplastic polymer and a cover slide glass.

The composition of the electrolytes studied in this work is shown in Table 2. Only the solvent composition is varied, and both redox pair and additives are kept the same for all studied devices.

Electrolyte	Solvent (v/v,%)	Solutes
Acn	100% Acetonitrile	0.1M I <sub>2</sub> + 1M BMII + 0.05M LiI + 0.5M TBP + 0.1M GuSCN
Imid25/Pyr25	75% Acn + 25% RTIL	
Imid50/Pyr50	50% Acn + 50% RTIL	
Imid75/Pyr75	25% Acn + 75% RTIL	
Imid/Pyr	100% RTIL	

**Table 2.** Composition of the electrolytes studied in this work. (I<sub>2</sub>: Iodine (99.5%, Fluka), LiI: Lithium iodide (99%, Aldrich), BMII: 1-butyl-3-methylimidazolium iodide (99%, Aldrich), TBP: 4-tert-butylpyridine (96%, Aldrich), GuSCN: Guanidine thiocyanate (99%, Aldrich), Acn: Acetonitrile (99.9%, Panreac), Imid: 1-Ethyl-3-Methylimidazolium bis(trifluoromethanesulfonyl)imide (99.9%, Solvionic), Pyr: 1-Buthyl-1-Methylpyrrolidinium bis(trifluoromethanesulfonyl)imide (99.9%, Solvionic).

### Characterization of devices

The devices were characterized using a solar simulator with AM 1.5G filter (ABET). The light intensity was calibrated to the standard value of 1 sun (100 mW/cm<sup>2</sup>) using a reference solar cell with temperature output (Oriel, 91150). The current-voltage characteristics were determined by applying an external potential bias to the cell and measuring the photocurrent using an Autolab/PGSTAT302N potentiostat. Open-circuit Voltage Decay measurements (OCVD) were made by keeping the solar cell at open-circuit at 1-sun and registering the voltage transient after interrupting the illumination.

Electrochemical Impedance Spectroscopy (EIS), Intensity Modulated Photovoltage Spectroscopy (IMVS), Intensity Modulated Photocurrent Spectroscopy (IMPS) and Open-Circuit Voltage Decay (OCVD) were utilized to study electron transport, recombination, chemical capacitance and to extract electron lifetimes.<sup>48,57</sup> The illumination for the small perturbation (frequency response) techniques was provided by a 540 nm light emitting diode (LUXEON). A response analyzer module (PGSTAT302N/FRA2, Autolab) was utilized to analyze the frequency response of the devices. EIS measurements were carried out under a varying bias potential and a fixed illumination (related to the open-circuit voltage) provided by the light emitting diode. The bias potential was corrected for voltage drop due to series resistance. A 10 mV perturbation in the 10<sup>5</sup>-10<sup>2</sup> Hz range was utilized to obtain the spectra. IMVS and IMPS measurements were carried out by coupling the PGSTAT302N/FRA2 module to the light emitting diode. This makes it possible to probe the devices at different positions of the Fermi level in the semiconductor. In all cases the samples were illuminated from the dye-coated TiO<sub>2</sub> electrode side.

IMVS measurements were performed at open circuit in the 10<sup>4</sup>-10<sup>1</sup> Hz range and IMPS measurements at short-circuit in the 10<sup>4</sup> to 10<sup>3</sup> Hz range with a light perturbation corresponding to 10% of the DC background illumination intensity. The NOVA 1.7 software was used to generate and treat the IMVS data. Zview equivalent circuit modeling software (Scribner) was used to fit the EIS spectra, including the distributed element DX11 (transmission line model).<sup>29,30</sup> To obtain the Fermi Level shift between open-circuit and short-circuit condition,<sup>44</sup> short-circuit voltage ( $V_{sc}$ )<sup>46,51</sup> measurements were performed. For this purpose, the solar cell was first illuminated under short-circuit conditions at various light intensities. The diode was then turned off and the cell was switched to open circuit simultaneously. The voltage evolution was finally monitored by the potentiostat.

For “blank” cells containing just the different electrolytes sandwiched between two platinized FTOs, cyclic voltammograms (CV) were recorded at a scan rate of 20 mV·s<sup>-1</sup>. These measurements were utilized to obtain limited currents and ionic diffusion coefficients

### Acknowledgements

We thank and the *Ministerio de Educación, Cultura y Deporte* for a FPU fellowship and *Abengoa Research* for support via a framework collaboration agreement.

### Notes and references

† Electronic Supplementary Information (ESI) available: [S1: Jsc and Voc for all electrolytes normalized in N719-cells, S2: Current-voltage curves and Jsc and Voc for all electrolytes normalized in Z907-cells, S3: Equivalent circuit utilized to fit impedance data, S4: Chemical capacitance data as extracted from EIS measurement for N719-cells and Z907-cells, S5: Electron recombination resistance and electron lifetime data are extracted from EIS measurement for Z907-cells, S6: EIS Nyquist plots for cells with Imid and Pry-based electrolytes in N719-cells, S7: Electron lifetime data extracted by OCVD for Z907- cell with and without blocking layer, S8: Electron Length diffusion obtained from IMVS and IMPS for Imid75 and Pyr75 in N719-cells, S9: Electron recombination resistance for N719 and Z907-cells]. See DOI: 10.1039/b000000x/

1. B. O'Regan and M. Grätzel, *Nature*, 1991, **353**, 737–740.
2. M. Grätzel, *Acc. Chem. Res.*, 2009, **42**, 1788–1798.
3. B. E. Hardin, H. J. Snaith, and M. D. McGehee, *Nat Photon*, 2012, **6**, 162–169.
4. H. J. Snaith, *J. Phys. Chem. Lett.*, 2013, **4**, 3623–3630.
5. J. R. Jennings, Y. Liu, Q. Wang, S. M. Zakeeruddin, and M. Grätzel, *Phys. Chem. Chem. Phys.*, 2011, **13**, 6637–6648.
6. S.-R. Jang, K. Zhu, M. J. Ko, K. Kim, C. Kim, N.-G. Park, and A. J. Frank, *ACS Nano*, 2011, **5**, 8267–8274.
7. Y. Liu, J. R. Jennings, S. M. Zakeeruddin, M. Grätzel, and Q. Wang, *J. Am. Chem. Soc.*, 2013, **135**, 3939–3952.
8. Y. Liu, J. R. Jennings, Y. Huang, Q. Wang, S. M. Zakeeruddin, and M. Grätzel, *J. Phys. Chem. C*, 2011, **115**, 18847–18855.
9. S. Mathew, A. Yella, P. Gao, R. Humphry-Baker, CurchodBasile F. E., N. Ashari-Astani, I. Tavernelli, U. Rothlisberger, NazeeruddinMd. Khaja, and M. Grätzel, *Nat Chem*, 2014, **6**, 242–247.

10. F. Fabregat-Santiago, J. Bisquert, E. Palomares, L. Otero, D. B. Kuang, S. M. Zakeeruddin, and M. Grätzel, *J. Phys. Chem. C*, 2007, **111**, 6550–6560.
11. D. Shi, N. Pootrakulchote, R. Li, J. Guo, Y. Wang, S. M. Zakeeruddin, M. Grätzel, and P. Wang, *J. Phys. Chem. C*, 2008, **112**, 17046–17050.
12. J. Idígoras, L. Pellejà, E. Palomares, and J. A. Anta, *J. Phys. Chem. C*, 2014, **118**, 3878–3889.
13. J. Bisquert, F. Fabregat-Santiago, I. Mora-Seró, G. Garcia-Belmonte, and S. Giménez, *J. Phys. Chem. C*, 2009, **113**, 17278–17290.
14. Q. Wang, S. Ito, M. Grätzel, F. Fabregat-Santiago, I. Mora-Sero, J. Bisquert, T. Bessho, and H. Imai, *J. Phys. Chem. B*, 2006, **110**, 25210–25221.
15. J. Bisquert and R. Marcus, Springer Berlin Heidelberg, 2013, pp. 1–71.
16. R. A. Marcus, *J. Chem. Phys.*, 1956, **24**, 966–978.
17. J. P. Gonzalez-Vazquez, G. Oskam, and J. A. Anta, *J. Phys. Chem. C*, 2012, **116**, 22687–22697.
18. J. W. Ondersma and T. W. Hamann, *J. Am. Chem. Soc.*, 2011, **133**, 8264–8271.
19. Y. Liu, A. Hagfeldt, X.-R. Xiao, and S.-E. Lindquist, *Sol. Energy Mater. Sol. Cells*, 1998, **55**, 267–281.
20. C. A. Kelly, F. Farzad, D. W. Thompson, J. M. Stipkala, and G. J. Meyer, *Langmuir*, 1999, **15**, 7047–7054.
21. S. Nakade, T. Kanzaki, W. Kubo, T. Kitamura, Y. Wada, and S. Yanagida, *J. Phys. Chem. B*, 2005, **109**, 3480–3487.
22. S. Pelet, J.-E. Moser, and M. Grätzel, *J. Phys. Chem. B*, 2000, **104**, 1791–1795.
23. S. Kambe, S. Nakade, Y. Wada, T. Kitamura, and S. Yanagida, *J Mater Chem*, 2002, **12**, 723–728.
24. S. Nakade, S. Kambe, T. Kitamura, Y. Wada, and S. Yanagida, *J. Phys. Chem. B*, 2001, **105**, 9150–9152.
25. Z. Yu, N. Vlachopoulos, A. Hagfeldt, and L. Kloo, *RSC Adv*, 2013, **3**, 1896–1901.
26. W. Kubo, S. Kambe, S. Nakade, T. Kitamura, K. Hanabusa, Y. Wada, and S. Yanagida, *J. Phys. Chem. B*, 2003, **107**, 4374–4381.
27. A. Noda, K. Hayamizu, and M. Watanabe, *J. Phys. Chem. B*, 2001, **105**, 4603–4610.
28. D. B. Kuang, C. Klein, S. Ito, J. E. Moser, R. Humphry-Baker, N. Evans, F. Durliaux, C. Graetzel, S. M. Zakeeruddin, and M. Graetzel, *Adv. Mater.*, 2007, **19**, 1133–1137.
29. J. Bisquert, *J. Phys. Chem. B*, 2002, **106**, 325–333.
30. F. Fabregat-Santiago, J. Bisquert, G. Garcia-Belmonte, G. Boschloo, and A. Hagfeldt, *Sol. Energy Mater. Sol. Cells*, 2005, **87**, 117–131.
31. P. J. Cameron and L. M. Peter, *J. Phys. Chem. B*, 2005, **109**, 7392–7398.
32. J. A. Anta, J. Idígoras, E. Guillen, J. Villanueva-Cab, H. J. Mandujano-Ramirez, G. Oskam, L. Pelleja, and E. Palomares, *Phys Chem Chem Phys*, 2012, **14**, 10285–10299.
33. J. Bisquert and I. Mora-Seró, *J. Phys. Chem. Lett.*, 2010, **1**, 450–456.
34. J. Bisquert, *Phys. Chem. Chem. Phys.*, 2003, **5**, 5360–5364.
35. M. Ansari-Rad, Y. Abdi, and E. Arzi, *J. Phys. Chem. C*, 2012, **116**, 10867–10872.
36. G. Boschloo and A. Hagfeldt, *Acc. Chem. Res.*, 2009, **42**, 1819–1826.
37. J. Rowley and G. J. Meyer, *J. Phys. Chem. C*, 2009, **113**, 18444–18447.
38. H. C., LIN Zhen, WU Kejun, XU Guohua ZHOU Ying, *Chin. J. Chem. Eng.*, 2014, **22**, 79.
39. E. W. Castner, J. F. Wishart, and H. Shirota, *Acc. Chem. Res.*, 2007, **40**, 1217–1227.
40. J. R. Jennings, F. Li, and Q. Wang, *J. Phys. Chem. C*, 2010, **114**, 14665–14674.
41. J. R. Jennings and Q. Wang, *J. Phys. Chem. C*, 2010, **114**, 1715–1724.
42. M. Ansari-Rad, Y. Abdi, and E. Arzi, *J. Appl. Phys.*, 2012, **112**, -.
43. G. Boschloo, E. A. Gibson, and A. Hagfeldt, *J. Phys. Chem. Lett.*, 2011, **2**, 3016–3020.
44. L. M. Peter, *J. Phys. Chem. C*, 2007, **111**, 6601–6612.
45. J. P. Gonzalez-Vazquez, J. A. Anta, and J. Bisquert, *J. Phys. Chem. C*, 2010, **114**, 8552–8558.
46. E. Guillén, L. M. Peter, and J. A. Anta, *J. Phys. Chem. C*, 2011, **115**, 22622–22632.
47. J. R. Jennings and L. M. Peter, *J. Phys. Chem. C*, 2007, **111**, 16100–16104.
48. J. Halme, *Phys. Chem. Chem. Phys. PCCP*, 2011, **13**, 12435–12446.
49. L. Dloczik, O. Ieperuma, I. Lauermaann, L. M. Peter, E. A. Ponomarev, G. Redmond, N. J. Shaw, and I. Uhlendorf, *J. Phys. Chem. B*, 1997, **101**, 10281–10289.
50. J. van de Lagemaat and A. J. Frank, *J. Phys. Chem. B*, 2000, **104**, 4292–4294.
51. G. Boschloo and A. Hagfeldt, *J. Phys. Chem. B*, 2005, **109**, 12093–12098.
52. L. M. Peter and K. G. U. Wijayantha, *Electrochimica Acta*, 2000, **45**, 4543–4551.
53. J. A. Anta, I. Mora-Sero, T. Dittrich, and J. Bisquert, *Phys. Chem. Chem. Phys.*, 2008, **10**, 4478–4485.
54. J. Bisquert, *J. Phys. Chem. B*, 2004, **108**, 2323–2332.
55. V. Sivaram, J. Kirkpatrick, and H. Snaith, *J. Appl. Phys.*, 2013, **113**, -.
56. A. Reynal, A. Forneli, and E. Palomares, *Energy Env. Sci*, 2010, **3**, 805–812.
57. A. Zaban, M. Greenshtein, and J. Bisquert, *Chemphyschem*, 2003, **4**, 859–864.